arXiv:2202.02149v1 [cs.CV] 4 Feb 2022

Edge-Selective Feature Weaving for Point Cloud Matching

Rintaro Yanagi[1,2], Atsushi Hashimoto[2], Shusaku Sone[2,3], Naoya Chiba[2,4], Jiaxin Ma[2], and Yoshitaka Ushiku[4]
Hokkaido Univ.[1], OMRON SINIC X Corp.[2], OMRON[3], Whichever University[4]
yanagi@lmd.ist.hokudai.ac.jp, atsushi.hashimoto@sinicx.com, Shusaku.Sone@omron.com
chiba@nchiba.net, jiaxin.ma@sinicx.com, contact@yoshitakaushiku.net

Abstract

This paper tackles the problem of accurately matching the points of two 3D point clouds. Most conventional methods improve their performance by extracting representative features from each point via deep-learning-based algorithms. On the other hand, the correspondence calculation between the extracted features has not been examined in depth, and non-trainable algorithms (e.g. the Sinkhorn algorithm) are frequently applied. As a result, the extracted features may be forcibly fitted to a non-trainable algorithm. Furthermore, the extracted features frequently contain stochastically unavoidable errors, which degrades the matching accuracy. In this paper, instead of using a non-trainable algorithm, we propose a differentiable matching network that can be jointly optimized with the feature extraction procedure. Our network first constructs graphs with edges connecting the points of each point cloud and then extracts discriminative edge features by using two main components: a shared set-encoder and an edge-selective cross-concatenation. These components enable us to symmetrically consider two point clouds and to extract discriminative edge features, respectively. By using the extracted discriminative edge features, our network can accurately calculate the correspondence between points. Our experimental results show that the proposed network can significantly improve the performance of point cloud matching. Our code is available at https://github.com/yanarin/ESFW

1. Introduction

Matching of two sample elements is a fundamental research topic in the field of computer vision [10, 17, 45]. Among various matching topics, 3D point cloud registration has been an essential, challenging task with the recent spread of 3D sensing technologies and 3D point cloud applications [10,45] (e.g., autonomous driving [2] and immersive communications [6]). The goal of most 3D point cloud registration methods is to find the correspondences between the points of two point clouds. Accurate 3D point cloud registration enables further development in downstream tasks such as motion transfer [31], shape editing [22], and object localization for industrial robots [4].

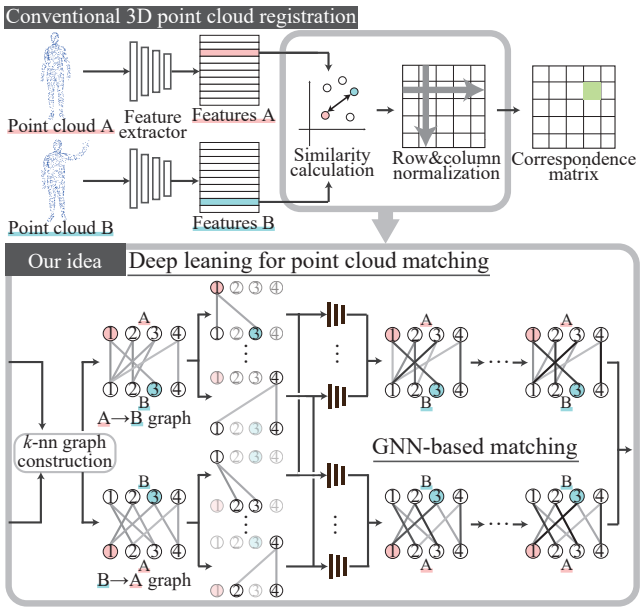

Figure 1. Concept of the proposed network for 3D point cloud registration. Our proposed network can be jointly optimized with the feature extractor network to achieve robustness against errors in the extracted features and to maximize the performance of the feature extractor.

The main process of 3D point cloud registration can be roughly divided into two steps: feature extraction from each point and correspondence matrix construction. Most traditional methods [3, 35, 41, 44] focus mainly on how to extract representative features from each point by using non-trainable algorithms such as keypoint detectors and local geometric descriptors. With the recent increase in data availability, deep neural networks (DNNs) have been widely adopted for feature extraction [27, 36], and they improve the matching performance significantly. Specifically, an unsupervised 3D point cloud registration method

called CorrNet3D was proposed to reduce the cost of collecting annotated data, and it has achieved state-of-the-art performance [44]. Although the rough matching of two point clouds has become possible with the DNN-based registration methods focusing on feature extraction, the finer matching is still a challenge because the correspondence matrix is adversely affected by stochastically unavoidable errors.

When the point clouds do not include any missing points (i.e. occlusions), it is desirable in 3D point cloud registration for the correspondence matrix to be binary and orthogonal [3, 35, 41, 44]. The DNN-based registration methods generally calculate the pairwise similarities between the extracted features of each point, and the resulting similarity matrix is then converted to the correspondence matrix via the Sinkhorn algorithm [24], which ideally constructs a binary, orthogonal matrix. In practice, however, stochastically unavoidable errors in the extracted features causes errors in the pairwise similarities [14, 15], which are detrimental to accurate construction of the correspondence matrix. Moreover, such forcible adjustments can limit the performance of the feature extractor [26]. Accordingly, for advancing the 3D point cloud registration methods by maximizing the feature extraction performance, a trainable matching architecture that can be jointly optimized with the feature extractor is required.

In this paper, we propose a differentiable matching network that can be jointly optimized with the feature extractor. Specifically, by adopting a graph neural network [37], we construct an edge-selective feature weaving (ESFW) module that can discriminatively analyze the relationships between the points across the point clouds. This concept is illustrated in Fig. 1. First, our ESFW module constructs graphs with edges connecting the points of each point cloud. Then, our ESFW module extracts discriminative edge features by using two graph neural network-based components: a shared set-encoder and an edge-selective cross-concatenation. The shared set-encoder enables us to deeply stack graph neural networks for discriminative extraction of edge features, while the edge-selective cross-concatenation enables us to handle mutual point cloud information bidirectionally. Finally, by constructing a correspondence matrix based on the extracted discriminative edge features, our network accurately performs the finer matching.

The contributions of this paper are summarized as follows.

Joint optimization of feature extraction and matching
To achieve robustness against errors in the extracted features and to maximize the performance of the feature extractor, we introduce a differentiable graph neural network that is specialized for point cloud matching.

Designing network architecture for the finer matching
To achieve the finer matching, we carefully design our ESFW module to discriminatively analyze the relationships between the points of each point cloud.

Experimental verification
We experimentally confirm that the performance of the state-of-the-art method is significantly improved on both rigid and non-rigid datasets in both supervised and unsupervised settings.

2. Related works

2.1. Rule-based registration algorithm

For 3D point cloud registration, the pioneering works sought to extract hand-crafted features and search for the nearest neighbor point [12, 32, 39, 46, 46]. Most such algorithms including Spin Image [12], ISS [46], SHOT [32], RCS [39], and TOLDI [40], first calculate a local reference frame (LRF). The LRF enables encoding of the 3D spatial information and makes the hand-crafted feature extractor rotation invariant. Then, via the LRF, these algorithms extract the features of each key-point and match the nearest neighbor points. For accurate matching of the extracted features, the nearest-neighbor distance ratio (NNDR) [13] is a widely known algorithm. In the NNDR, the nearest and second-nearest neighbors of each extracted feature are calculated. If the ratio of the distances between the nearest and second-nearest neighbors is below a threshold, the nearest neighbor is treated as a correspondence point. Although the matching performance has been improved with these hand-crafted matching algorithms, point cloud resolutions, noise, clutter, and occlusions suppress the performance [7].

2.2. Deep learning-based registration algorithm

The recent growth in deep learning methods has led to various approaches for application of DNNs to 3D point cloud registration [1, 30, 35, 41, 44, 45]. These approaches can be roughly divided into two types: those that handle the entire scene simultaneously, and those that are based on local feature-matching results. While the former approach enables global registration, it is difficult to apply to large point clouds or scenes with occlusions. Our work thus follows the latter approach, which can extract local features and perform end-to-end 3D point cloud registration by introducing a trainable matching network.

Within the latter approach, many methods extract representative features from each point and search for corresponding points by calculating the distances between point features [8, 9]. In the early years of research on this approach, most methods converted point clouds to other representation styles such as RGB-D images and then extracted

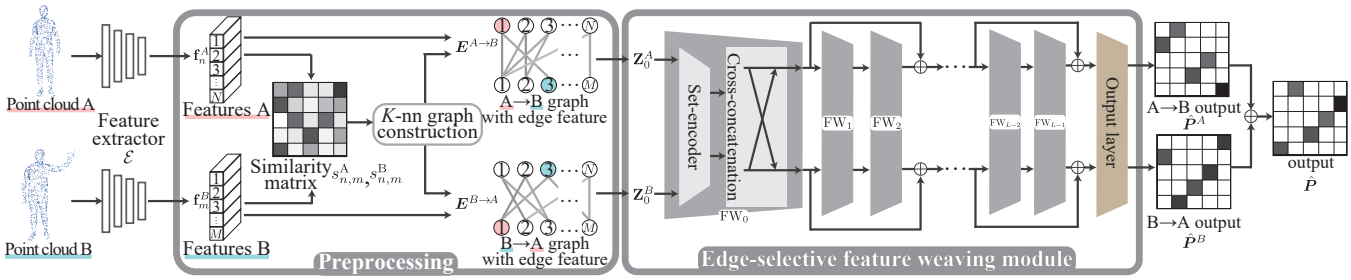

Figure 2. Overview of the proposed method. At first, the proposed method constructs a directional bipartite graph. Then our method extracts the discriminative edge features based on two main components specialized for matching: a shared set-encoder and an edge-selective cross-concatenation.

local features with a well-established 2D or 3D convolutional neural network (CNN) [5, 23, 43]. For example, [5] projected a 3D point cloud to RGB-D images and then extracted features by using a 2D CNN. Among more recent methods, PointNet [27] and DeepSets [42] can directly process raw unstructured point clouds. These methods demonstrate that permutation invariance of the neural network can be introduced by using symmetric functions, and the resulting feature extractors are used for point cloud matching. Although these feature extraction methods have greatly advanced point cloud processing [28, 36, 38], they can only be applied for matching between individual points [30], which makes it difficult to find the best combination between points.

To achieve point matching on a many-to-many basis, recent methods construct a similarity matrix for extracted point feature and then convert the similarity matrix to a correspondence matrix via the Sinkhorn algorithm [41, 44]. Here, the Sinkhorn algorithm helps find the best combination between points by iteratively and alternatively performing the softmax operation column-wise and row-wise [24]. Among these many-to-many methods, the CorrNet3D model achieves state-of-the-art performance in both supervised and unsupervised settings by using an improved version of the Sinkhorn algorithm called the DeSmooth module [44]. Although these methods can handle point matching on a many-to-many basis, stochastically unavoidable errors in the extracted features causes errors in the pairwise similarities, which make it difficult to accurately construct the correspondence matrix [14, 15]. To overcome this difficulty, and provide a new idea for many-to-many point matching, our proposed network learns feature extraction and point matching simultaneously via a differentiable matching network.

3. Edge-selective feature weaving

Let $\boldsymbol{X}^A$ and $\boldsymbol{X}^B$ be point clouds with sizes N and M, respectively. We refer to the n-th element in $\boldsymbol{X}^A$ as $\mathbf{x}^A_n \in \mathcal{R}^{D_x}$ $(n = 1, \ldots, N)$ and the m-th element in $\boldsymbol{X}^B$ as $\mathbf{x}^B_m \in \mathcal{R}^{D_x}$ $(m = 1, \ldots, M)$, where $D_x = 3$ when we represent a point by its position in 3D space, for example. Point cloud matching is defined as the task of predicting a correspondence matrix $\boldsymbol{P} = [p_{n,m}]_{N\times M}$ from the inputs $\boldsymbol{X}^A$ and $\boldsymbol{X}^B$.

Figure 2 shows an overview of our approach. The goal is to make the correspondence calculation trainable with a certain network $\mathcal{M}$. Hence, we assume a feature extractor $\mathcal{E} : \mathbf{x} \to \mathbf{f}$ $(\mathbf{f} \in \mathcal{R}^{D_f})$, where the features $\mathbf{f}^A = \mathcal{E}(\mathbf{x}^A)$ and $\mathbf{f}^B = \mathcal{E}(\mathbf{x}^B)$ are fed to $\mathcal{M}$ to estimate $\boldsymbol{P}$. By jointly optimizing $\mathcal{E}$ and $\mathcal{M}$, we seek a better solution than those obtained with a non-trainable correspondence calculation. In the following subsections, we describe the details of the preprocessing for $\mathcal{M}$ (Subsec. 3.1) and the network architecture of $\mathcal{M}$ (Subsec. 3.2).

3.1. Preprocessing

For each $\mathbf{x}^A_n$, $\mathcal{M}$ works to find a correct match in $\boldsymbol{X}^B$ (and similarly, in $\boldsymbol{X}^A$ for each $\mathbf{x}^B_m$). Let us consider a directional bipartite graph $G(\boldsymbol{V}^A, \boldsymbol{V}^B, \boldsymbol{E}^{A\to B}, \boldsymbol{E}^{B\to A})$ where $\boldsymbol{V}^A = \{\mathbf{f}^A_n | n = 1, \ldots, N\}$ and $\boldsymbol{V}^B = \{\mathbf{f}^B_m | m = 1, \ldots, M\}$ are two sides of vertices, $\boldsymbol{E}^{A\to B}$ is the set of edges from side A to B, and $\boldsymbol{E}^{B\to A}$ is the set of edges from B to A. For simplicity, we only give the formulae for A here; the same formulae are defined symmetrically for B. To prune matching candidates that have no chance to be matched , we propose to simply select candidate edges from $\boldsymbol{E}^{A\to B}$ by the K-nearest neighbors algorithm.

Our concrete implementation of this calculation is as follows. Since we implement our method on CorrNet3D, we borrow its similarity definition. For each pair $\{\mathbf{f}^A_n, \mathbf{f}^B_m\}$, we calculate the similarity $s^A_{n,m}$ as

$$s^{\mathrm{A}}_{n,m} = \frac{1}{\|\mathbf{f}^A_n - \mathbf{f}^B_m\|_2}. \tag{1}$$

In terms of this similarity, we find the top K most similar neighbors, denoted as $\mathcal{N}(n)$, for each n-th point and we add $\{\{n, m\} | m \in \mathcal{N}(n)\}$ to $\boldsymbol{E}^{A\to B}$.

Finally, using $\boldsymbol{E}^{A\to B}$ and $\boldsymbol{E}^{B\to A}$, we generate $\mathbf{z}^A_{0,n,m}$, an input to the first (0-th) layer of $\mathcal{M}$ that represents an edge $\{n, m\} \in \boldsymbol{E}^{A\to B}$. Then, with a concatenating operation

$\mathrm{cat}(\cdot)$, we define the feature as

$$\mathbf{z}^A_{0,n,m} = \mathrm{cat}(\mathbf{f}^A_n, (s^A_{n,m}), \mathbf{f}^B_m). \tag{2}$$

3.2. Network architecture

Let $\mathbf{Z}^A_0$ denote the set of input features $\{\mathbf{z}^A_{0,n,m} | \{n,m\} \in \boldsymbol{E}^{A\to B}\}$. We design $\mathcal{M}$ as a network whose input is $\{\mathbf{Z}^A_0, \mathbf{Z}^B_0\}$ and whose output is an estimate of the correspondence matrix $\hat{\boldsymbol{P}}$. When $\mathcal{M}$ is trained ideally, row-wise and column-wise argmax operations should yield an identical result, which is the optimal match.

To implement this matching network architecture, we propose an edge-selective feature weaving layer inspired from PointNet [27] and DeepSets [42]. Let $\mathrm{FW}_l : \{\mathbf{Z}^A_l, \mathbf{Z}^B_l\} \to \{\mathbf{Z}^A_{l+1}, \mathbf{Z}^B_{l+1}\}$ be the l-th feature weaving layer. Here, $\mathbf{Z}^A_l = \{\mathbf{z}^A_{l,n,m} | \{n,m\} \in \boldsymbol{E}^{A\to B}\}$ is a set of intermediate representations when $l > 0$. We organize $\mathcal{M}$ by stacking $L-1$ feature weaving layers ($l = 0, \ldots, L-1$) and one output layer.

The feature weaving layer has two main components: a shared set-encoder and an edge-selective cross-concatenation. The shared set-encoder serves to emphasize the relative characteristics of each edge among the adjacent edges. The edge-selective cross-concatenation is applied to the output of the shared set-encoder to propagate the mutual stream information to the other stream. At the output layer, we merge the outputs of the shared set-encoder into $\hat{\boldsymbol{P}}$ instead of applying the cross-concatenation.

The shared set-encoder seeks to extract representative edge features for matching. It is desirable that edge features are highly discriminative for accurate, stable matching of two elements, and then it is necessary to analyze each edge feature via the deep network while considering the other edge features. PointNet [27] and DeepSets [42] provide a suitable structure for this purpose, a combination of max-pooling with two linear operations. However, these average aggregation process is also known to smooth edge features as the network gets deeper [19, 25]. Accordingly, to alleviate this effect and extract discriminative features with the deep network, we extend the conventional graph neural network process.

Specifically, we first extract edge features via a trainable linear layer $\phi^1_l(\cdot)$ and max-pooling $\max(\cdot)$ as follows:

$$\mathbf{h}^A_{l,n} = \max_{m_k \in \mathcal{N}(n)} (\phi^1_l(\mathbf{z}^A_{l,n,m_k})). \tag{3}$$

Hence, $\mathbf{h}^A_{l,n}$ is expected to aggregate all the specific characteristics of matching candidates. Next, we concatenate $\mathbf{h}^A_{l,n}$ to the feature of each edge $\mathbf{z}^A_{l,n,m}$ and apply another linear layer $\phi^2_l(\cdot)$ to compare them as follows:

$$\mathbf{g}^A_{l,n,m} = \mathrm{act}(\mathrm{BN}(\phi^2_l(cat(\mathbf{z}^A_{l,n,m}, \mathbf{h}^A_{l,n})))), \tag{4}$$

where $\mathrm{act}(\cdot)$ and $\mathrm{BN}(\cdot)$ represent pReLU activation and batch normalization, respectively. Here, $\mathbf{g}^A_{l,n,m}$ is a D_g-dimensional feature. By feed-forwarding $\mathbf{g}^A_{l,n,m}$ without averaging, $\mathcal{M}$ can compare the candidates precisely.

The edge-selective cross-concatenation seeks to propagate the mutual stream information to the other stream. To accurately match the elements of two samples, it is important to collaboratively consider valuable edges in the other stream. We achieve this by concatenating the features in a stream-crossing manner (A to B and B to A).

In principle, the combined features should be relevant to each edge, and then the concatenation of $\mathbf{g}^A_{l,n,m}$ and $\mathbf{g}^B_{l,m,n}$ is a straightforward choice. However, because the similarity matrix $\boldsymbol{S} = [s_{n,m}]_{N\times M}$ is generally not symmetric, the K-nearest selection also yields an asymmetric choice of $\boldsymbol{E}^{A\to B}$ and $\boldsymbol{E}^{B\to A}$; that is, $\mathbf{g}^B_{l,m,n}$ is not always calculated in stream B. In that case, we have the two options, eliminating such edges from candidates or preparing a substitution of $\mathbf{g}^B_{l,m,n}$ anyway. Since the former option could eliminate all candidates in the worst case, we use the latter option, and we specify the substitute for an absent $\mathbf{g}^B_{l,m,n}$ as the mean of the candidates $\mathcal{N}(n)$. Overall, the edge-selective cross-concatenation is defined as

$$\mathbf{z}^A_{l+1,n,m} = \mathrm{cat}(\mathbf{g}^A_{l,n,m}, \mathbf{g'}^B_{l,n,m}), \tag{5}$$

$$\mathbf{g'}^B_{l,n,m} = \begin{cases} \mathbf{g}^B_{l,m,n} & \text{if } \{m,n\} \in \boldsymbol{E}^{B\to A} \\ \frac{1}{K} \sum_{m_k \in \mathcal{N}(n)} \mathbf{g}^B_{l,m_k,n} & \text{otherwise} \end{cases}, \tag{6}$$

where $\mathbf{z}^A_{l+1,n,m}$ is the output of FW_l, which is feed-forwarded to the next feature weaving layer FW_{l+1}.

Note that, to stack the feature weaving layers deeply, we include shortcut paths every two feature weaving layers to create a residual structure. For this purpose, we use an identical channel width D_z as the output of every feature weaving layer (i.e., $\mathbf{z}^A_{l,n,m} \in \mathcal{R}^{D_z}$ for $l = 1, \ldots, L$), where $D_z = 2D_g$.

The output layer finalizes $\mathbf{Z}^A_L$, the output of the $(L-1)$ stacked feature weaving layers, to be an estimate of the correspondence matrix $\hat{\boldsymbol{P}}$. This layer first applies the same calculation as in Eq. (3), and then calculates

$$\mathbf{g}^A_{L,n,m} = \mathrm{BN}(\phi^2_l(cat(\mathbf{z}^A_{L,n,m}, \mathbf{h}^A_{L,n}))). \tag{7}$$

This is almost the same as Eq. (4) but without activation. Batch normalization is necessary to prevent the output from falling into a trivial local minimum, which would yield quite small values at all points and make $\hat{\boldsymbol{P}}$ a uniform matrix.

Next, we calculate each element $\hat{p}^A_{n,m}$ in a matrix $\hat{\boldsymbol{P}}^A$ as follows:

$$\hat{p}^A_{n,m} = \begin{cases} \mathbf{g}^A_{L,n,m} & \text{if } \{n,m\} \in \boldsymbol{E}^{A\to B} \\ -\infty & \text{otherwise} \end{cases} \tag{8}$$

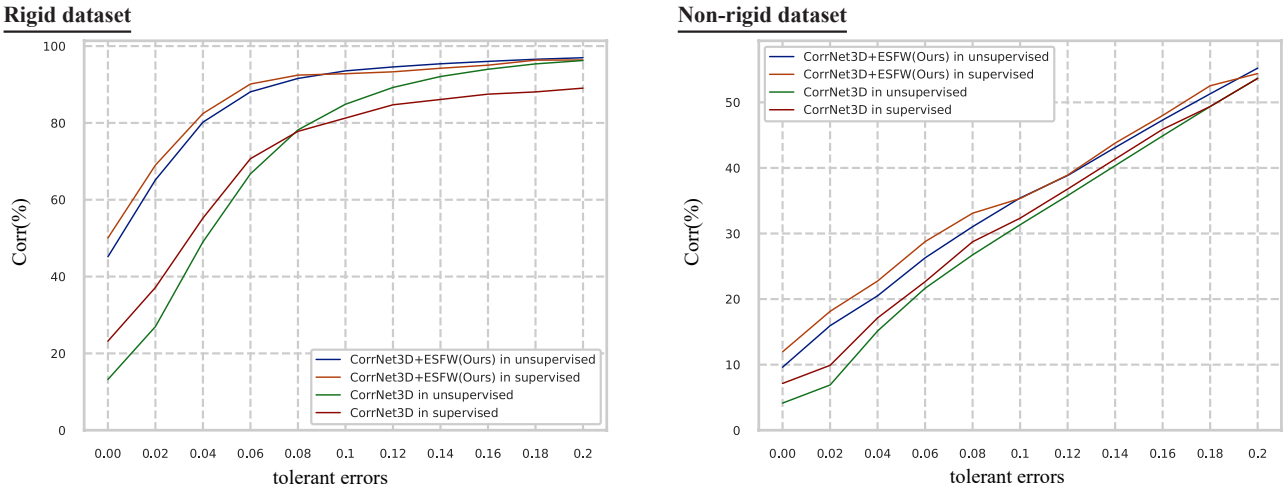

Figure 3. Experimental results on the rigid and non-rigid datasets. The vertical axis indicates the matching performance (Eq. 10), and the horizontal axis indicates the tolerant errors described in Subsec. 4.1.

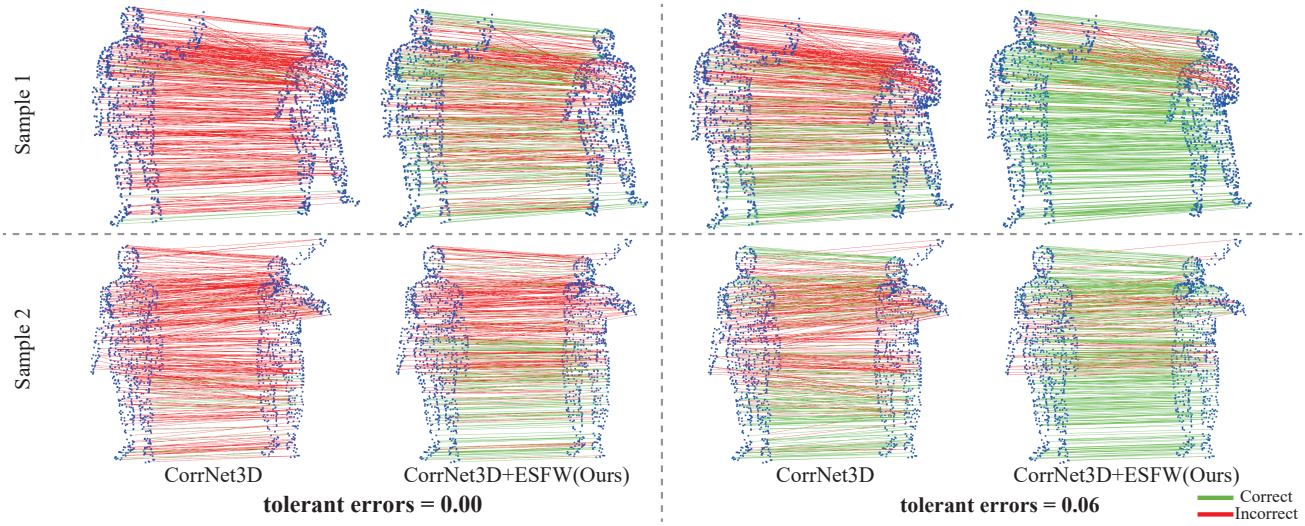

Figure 4. The samples of the experimental results with the non-rigid dataset in unsupervised setting. The green line shows the correctly matching pair, and the red line shows the incorrectly matching pair. Each sample is randomly selected for fair comparison, and we show correspondence relationships from random 600 points for visibility. Note that we select the same points in each method. The othere results can be seen in the supplemental materials.

By merging the two streams' outputs, we obtain the final output as

$$\hat{\boldsymbol{P}} = \frac{\hat{\boldsymbol{P}}^{A} + \hat{\boldsymbol{P}}^{B^{\top}}}{2}. \tag{9}$$

4. Experiments

To evaluate the effectiveness of our edge-selective feature weaving (ESFW) module, we conducted experiments with both supervised and unsupervised point cloud registration tasks. Because the CorrNet3D model obviously outperforms the other recent 3D point cloud registration methods on both rigid and non-rigid datasets in both supervised and unsupervised settings, we adopted it as a baseline. The performance of other methods can be seen in graphs of its paper [44].

4.1. Experimental settings

Dataset. Following the experiments in [44], we conducted experiments in both rigid and non-rigid settings. Note that, in each experiment, we used the data split provided by [44]. For the rigid setting, we used the Surreal dataset [33], which contains 230K point cloud samples for training and 100 samples for testing. The 230K point clouds were randomly paired into 115K training samples, and 100 test pairs were created by randomly rotating and translat-

ing the test samples. For the non-rigid setting, we used the Surreal dataset and the SHREC dataset [18] for training and test, which respectively contain 230K and 860 samples. The training samples were the same as in the rigid setting, while the 860 test samples were randomly combined into 430 test pairs. For all the above datasets, each point cloud contained 1024 points.

Evaluation metrics. For the evaluation metrics, following [44], we used the corresponding percentage (Corr) under various tolerant errors. The Corr and tolerant errors are defined as follows:

$$\text{Corr} = \frac{1}{N}||\boldsymbol{P} \odot \boldsymbol{P}^{\text{gt}}||_1, \tag{10}$$

$$\text{tolerant errors} = r/\text{dist}_{\text{max}}, \tag{11}$$

$$\text{dist}_{\text{max}} := \max\{||\boldsymbol{x}_i^{\text{A}} - \boldsymbol{x}_j^{\text{A}}||, \forall i, j\}, \tag{12}$$

where $\odot$, $\boldsymbol{P}^{\text{gt}}$, $||\cdot||_1$ and r respectively represent the Hadamard product, ground-truth correspondence matrix, L1-norm and tolerant radius.

Implementation details. In this experiment, we replaced the DeSmooth module in the CorrNet3D model with our ESFW module, which was optimized according to the loss function, as in CorrNet3D. For the parameters in the equations, we set $K = 128$, $D_f = 128$, $L = 10$ and $D_g = 16$. Also, following [44], we trained the model with the Adam optimizer, a learning rate of 1e-4, a batch size of 10 and 100 epochs. We implemented the model with the PyTorch framework on a Tesla V100 GPU.

4.2. Experimental results

Experimental results on rigid dataset. We show the experimental results on the rigid dataset in the "Rigid dataset" of Fig. 3. Here, the result labeled "CorrNet3D+ESFW in supervised (resp. unsupervised)" shows the matching performance of CorrNet3D with our ESFW module in the supervised (resp. unsupervised) setting. As shown in the figure, the CorrNet3D+ESFW model outperforms the baseline CorrNet3D model in both supervised and unsupervised settings. From these results, we confirmed that our ESFW module could significantly improve the performance of the CorrNet3D model simply by including it in the matching procedure. In other words, for the rigid point cloud matching, the trainable GNN-based function is more effective than the non-trainable function. Furthermore, the performance improvement especially for smaller tolerant errors reveals that our ESFW module discriminatively finds the corresponding point from similar points. From these results, the effectiveness of our ESFW module is confirmed in the rigid point cloud matching setting.

Experimental results on non-rigid dataset. Figure 3 also shows the experimental results on the non-rigid dataset. Again, the CorrNet3D+ESFW model outperforms the CorrNet3D model in both the supervised and unsupervised settings, which confirmed the effectiveness of our ESFW module in non-rigid point cloud matching setting. On the other hand, the performance improvement for smaller tolerant errors seems not as high as in the rigid case. We assume that these results are due to the difficulties of the non-rigid point cloud matching setting. For further performance improvement, investigation about sophisticated collaboration between the baseline model and ESFW module is required.

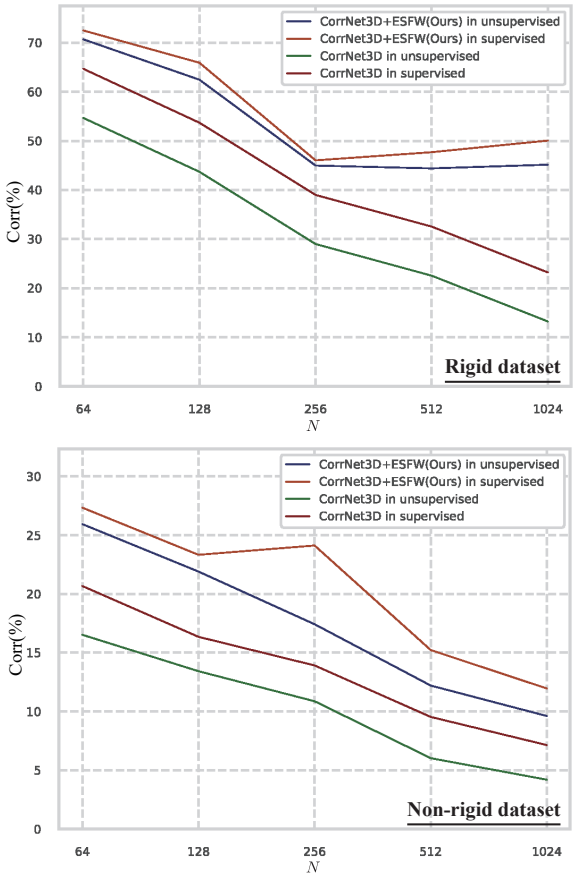

Figure 5. Experimental results from varying the hyperparameter N with the rigid and non-rigid datasets. The vertical axis indicates the matching performance (Eq. 10), and the horizontal axis indicates the hyperparameter N.

Qualitative results. We show the samples of the experimental results in Fig. 4. In each sample, the CorrNet3D+ESFW model can accurately match points compared with the CorrNet3D model. Furthermore, the results of the CorrNet3D+ESFW model in tolerant errors = 0.00 is similar to the results of the CorrNet3D model in tolerant errors = 0.06. From these results, it is considered that our ESFW module helps finer matching of CorrNet3D model.

4.3. Ablation study

For further understanding of our ESFW module, we extensively conducted various extensive ablation studies. Specifically, we examined the effects of the hyperparame-

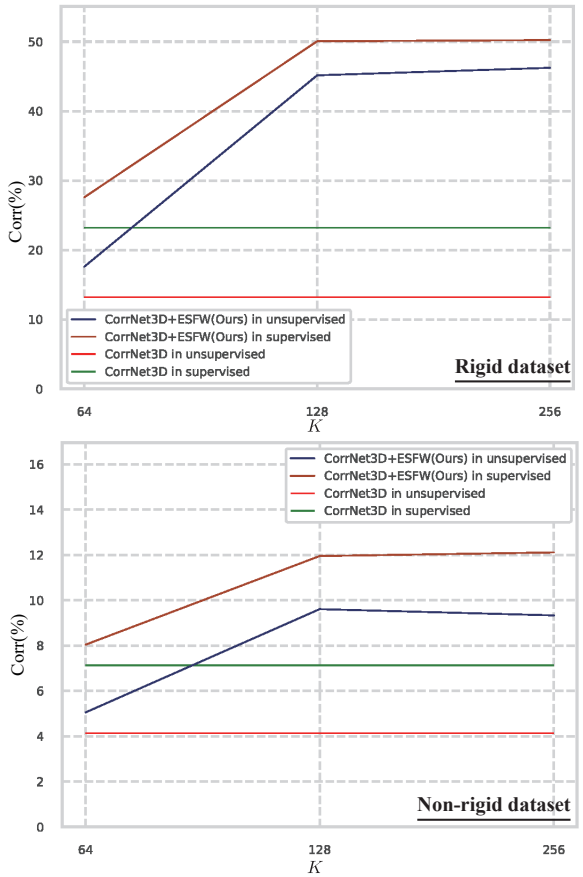

Figure 6. Experimental results from varying the hyperparameter K with the rigid and non-rigid dataset. The vertical axis indicates the matching performance (Eq. 10), and the horizontal axis indicates the hyperparameter K.

ters N, K, L, and D_g. Each experiment follows the same settings described in Subsec. 4.1, and we report the experimental results of changing each hyperparameter. Furthermore, we compared the matching performance with that of the CorrNet3D model in both the supervised and unsupervised settings. Because the CorrNet3D model does not include K, L, and D_g, these performances are plotted as horizontal lines. For the experiments with K, L, and D_g, we show the experimental results with the tolerant errors = 0.00.

Effect of N. The hyperparameter N represents the number of input points, and its value depends on the point cloud. To confirm the robustness of our ESFW module with respect to N, we conducted experiments with $N = 64$, 128, 256, 512, and 1024. In these experiments, we subsampled the point clouds by furthest point sampling.

Figure 5 shows the experimental results. For each N, the CorrNet3D+ESFW model outperforms the CorrNet3D model in both the supervised and unsupervised settings, which confirmed the robustness of our ESFW module with respect to N. On the other hand, we observed that the tendencies of each experimental result are differed according to the test dataset. For example, with $N > 256$, although the matching performances are not decreased in the rigid dataset, they are decreased on the non-rigid dataset. For practical application, further analysis is required to understand the differences between the datasets as the next step of our research.

Effects of K. The hyperparameter K represents the number of edges coming from each node. Accordingly, K affects memory usage, and it is desirable to adopt a smaller K. To examine the relationship between the matching performance and K, we conducted experiments with $K = 64$, $K = 128$, and $K = 256$.

Experimental results are shown in Fig. 6. As shown in Fig. 6, the performance of the CorrNet3D+ESFW model decreased with $K = 64$. These results reveal that our network is sensitive to the value of K, and we regard this as a limitation of our approach. On the other hand, such sensitivity to a hyperparameter can be observed universally in the field of point cloud processing [11, 20, 29], and we believe that this limitation should be tackled as a general challenge for the field.

Effects of L. The hyperparameter L represents the number of feature weaving layers in our ESFW module. To confirm that the ESFW module can extract valuable edge features while alleviating the smoothing problem (as described in "the shared set-encoder" of SubSec. 3.2), we conducted experiments with $L = 4$, $L = 6$, $L = 8$, and $L = 10$.

Experimental results are shown in Fig. 7. As shown in Fig. 7, the performance of the CorrNet3D+ESFW model improved in proportion to the number of feature weaving layers L. From these results, we confirmed that the ESFW module can extract valuable edge features while alleviating the smoothing problem. Furthermore, even with smaller L, the CorrNet3D+ESFW model outperforms the CorrNet3D model in both supervised and unsupervised settings. From these results, we further confirmed the effectiveness of our ESFW module towards the 3D point cloud registration.

Effects of D_g. The hyperparameter D_g represents the dimension of the extracted features in our network, and the number of trainable parameters also proportionately increases with D_g. Accordingly, D_g directly effects the memory usage, and it is desirable to adopt a smaller D_g. To examine the relationship between the matching performance and D_g, we conducted experiments with $D_g = 8$, $D_g = 16$, $D_g = 32$, and $D_g = 64$.

Experimental results are shown in Fig. 8. As shown in Fig. 8, the CorrNet3D+ESFW model achieves the best performance with $D_g = 16$ in both the supervised and unsupervised settings. From these results, we confirmed that adjustment of D_g leads to further performance improvement. It is considered that excessive and insufficient parameters respectively cause overfitting and underfitting in general neu-

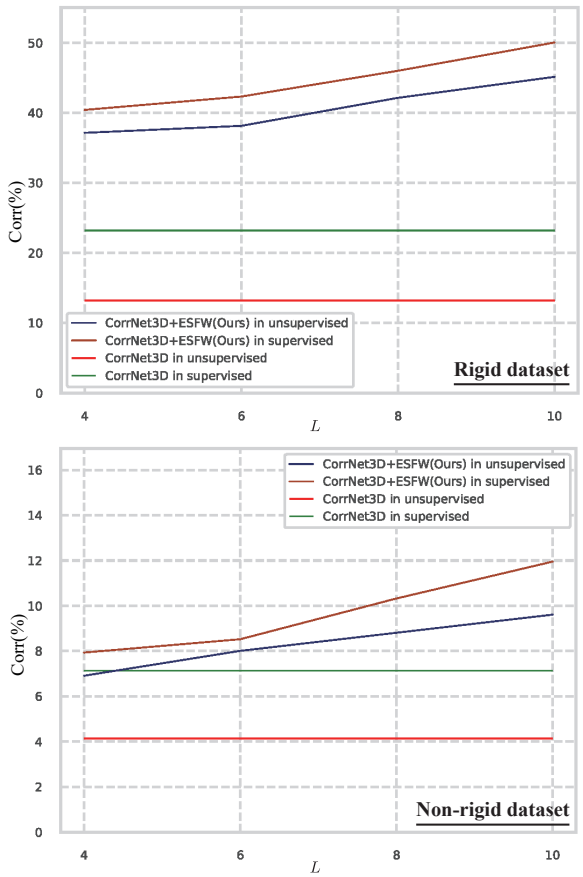

Figure 7. Experimental results from varying the hyperparameter L with the rigid and non-rigid dataset. The vertical axis indicates the matching performance (Eq. 10), and the horizontal axis indicates the hyperparameter L.

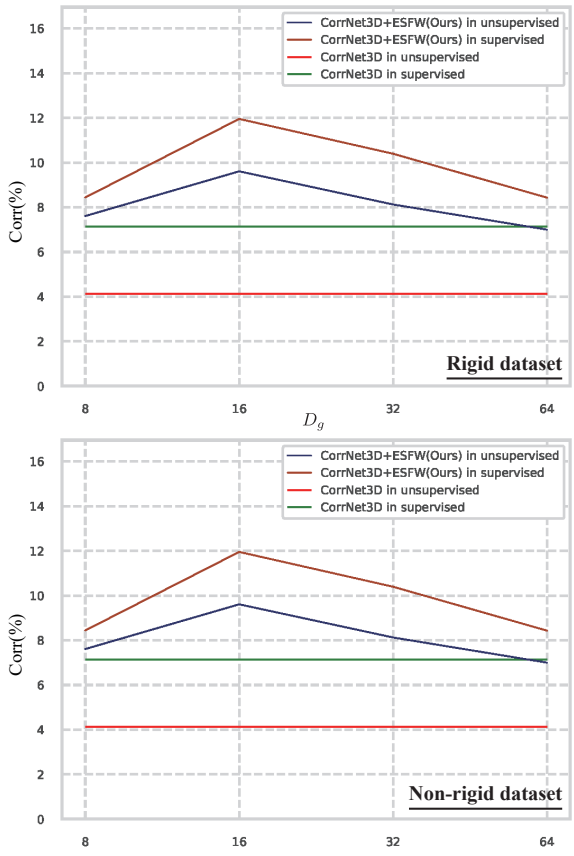

Figure 8. Experimental results from varying the hyperparameter D_g with the rigid and non-rigid dataset. The vertical axis indicates the matching performance (Eq. 10), and the horizontal axis indicates the hyperparameter D_g.

ral networks. On the other hand, for each D_g, the CorrNet3D+ESFW model outperforms the CorrNet3D model in both supervised and unsupervised settings. From these results, we confirmed the robustness with respect to D_g.

5. Limitation

The first remarkable limitation of our approach is the sensitivity to the hyperparameter K. As with the other point cloud processing methods [11,20,29], our ESFW module is also subject to negative effects in a particular hyperparameter setting. Specifically, as shown in Fig. 6, it is crucial to select a suitable value of K, which is the number of selected edges. Too small a K value can eliminate the edge toward the corresponding node, whereas too large a K value can lead to leave valueless edges. To overcome this limitation, further architectural improvements are needed.

The second limitation is memory usage as shown in point cloud processing [21, 34] and graph neural networks [16, 37]. Our ESFW module process graphs with edge information, and its memory usage thus becomes larger in proportion with the numbers of input points N and selected edges K. Because this limitation is closely related to the first limitation, it is important to consider an ideal architecture in terms of both limitations. Note that, since the selection of K edges is conducted based on the extracted features, we believe that the architecture should be considered not only for our ESFW module but also for the point cloud feature extractor.

6. Conclusion

In this paper, we have proposed a differentiable matching network for point cloud matching that can be jointly learned with the feature extraction procedure. Our experimental results demonstrate that our idea of joint optimization between feature extraction and point-to-point matching expands the limits of 3D point cloud registration and will cultivate further performance improvement. In addition to the 3D point cloud registration, the proposed network may also improve the performance of other matching tasks. In our future works, we will tackle both architecture improvement and verification on other tasks.

References

[1] Yasuhiro Aoki, Hunter Goforth, Rangaprasad Arun Srivatsan, and Simon Lucey. PointNetLK: Robust & efficient point cloud registration using pointnet. In *Proceedings of the IEEE/CVF Conference on Computer Vision and Pattern Recognition*, pages 7163–7172, 2019.

[2] Yaodong Cui, Ren Chen, Wenbo Chu, Long Chen, Daxin Tian, Ying Li, and Dongpu Cao. Deep learning for image and point cloud fusion in autonomous driving: A review. *IEEE Transactions on Intelligent Transportation Systems*, 2021.

[3] Nicolas Donati, Abhishek Sharma, and Maks Ovsjanikov. Deep geometric functional maps: Robust feature learning for shape correspondence. In *Proceedings of the IEEE/CVF Conference on Computer Vision and Pattern Recognition*, pages 8592–8601, 2020.

[4] Guoguang Du, Kai Wang, Shiguo Lian, and Kaiyong Zhao. Vision-based robotic grasping from object localization, object pose estimation to grasp estimation for parallel grippers: a review. *Artificial Intelligence Review*, 54(3):1677–1734, 2021.

[5] Gil Elbaz, Tamar Avraham, and Anath Fischer. 3D point cloud registration for localization using a deep neural network auto-encoder. In *Proceedings of the IEEE Conference on Computer Vision and Pattern Recognition*, pages 4631–4640, 2017.

[6] Guillaume Gamelin, Amine Chellali, Samia Cheikh, Aylen Ricca, Cedric Dumas, and Samir Otmane. Point-cloud avatars to improve spatial communication in immersive collaborative virtual environments. *Personal and Ubiquitous Computing*, pages 1–18, 2020.

[7] Yulan Guo, Mohammed Bennamoun, Ferdous Sohel, Min Lu, Jianwei Wan, and Ngai Ming Kwok. A comprehensive performance evaluation of 3D local feature descriptors. *International Journal of Computer Vision*, 116(1):66–89, 2016.

[8] Yulan Guo, Hanyun Wang, Qingyong Hu, Hao Liu, Li Liu, and Mohammed Bennamoun. Deep learning for 3D point clouds: A survey. *IEEE Transactions on Pattern Analysis and Machine Intelligence*, 2020.

[9] Xian-Feng Hana, Jesse S Jin, Juan Xie, Ming-Jie Wang, and Wei Jiang. A comprehensive review of 3D point cloud descriptors. *arXiv preprint arXiv:1802.02297*, 2, 2018.

[10] Xiaoshui Huang, Guofeng Mei, Jian Zhang, and Rana Abbas. A comprehensive survey on point cloud registration. *arXiv preprint arXiv:2103.02690*, 2021.

[11] Haiyong Jiang, Feilong Yan, Jianfei Cai, Jianmin Zheng, and Jun Xiao. End-to-end 3D point cloud instance segmentation without detection. In *Proceedings of the IEEE/CVF Conference on Computer Vision and Pattern Recognition*, pages 12796–12805, 2020.

[12] Andrew E Johnson and Martial Hebert. Using spin images for efficient object recognition in cluttered 3D scenes. *IEEE Transactions on Pattern Analysis and Machine Intelligence*, 21(5):433–449, 1999.

[13] Pedro R Mendes Júnior, Roberto M De Souza, Rafael de O Werneck, Bernardo V Stein, Daniel V Pazinato, Waldir R de Almeida, Otávio AB Penatti, Ricardo da S Torres, and Anderson Rocha. Nearest neighbors distance ratio open-set classifier. *Machine Learning*, 106(3):359–386, 2017.

[14] Zhao Kang, Yiwei Lu, Yuanzhang Su, Changsheng Li, and Zenglin Xu. Similarity learning via kernel preserving embedding. In *Proceedings of the AAAI Conference on Artificial Intelligence*, volume 33, pages 4057–4064, 2019.

[15] Zhao Kang, Chong Peng, and Qiang Cheng. Kernel-driven similarity learning. *Neurocomputing*, 267:210–219, 2017.

[16] Johannes Klicpera, Aleksandar Bojchevski, and Stephan Günnemann. Predict then propagate: Graph neural networks meet personalized pagerank. *arXiv preprint arXiv:1810.05997*, 2018.

[17] Chengcai Leng, Hai Zhang, Bo Li, Guorong Cai, Zhao Pei, and Li He. Local feature descriptor for image matching: A survey. *IEEE Access*, 7:6424–6434, 2018.

[18] Bo Li, Yijuan Lu, Chunyuan Li, Afzal Godil, Tobias Schreck, Masaki Aono, Martin Burtscher, Qiang Chen, Nihad Karim Chowdhury, Bin Fang, et al. A comparison of 3D shape retrieval methods based on a large-scale benchmark supporting multimodal queries. *Computer Vision and Image Understanding*, 131:1–27, 2015.

[19] Qimai Li, Zhichao Han, and Xiao-Ming Wu. Deeper insights into graph convolutional networks for semi-supervised learning. In *Proceedings of the AAAI Conference on Artificial Intelligence*, pages 3538–3545, 2018.

[20] Hao Liu, Yulan Guo, Yanni Ma, Yinjie Lei, and Gongjian Wen. Semantic context encoding for accurate 3D point cloud segmentation. *IEEE Transactions on Multimedia*, 2020.

[21] Jinxian Liu, Bingbing Ni, Caiyuan Li, Jiancheng Yang, and Qi Tian. Dynamic points agglomeration for hierarchical point sets learning. In *Proceedings of the IEEE/CVF International Conference on Computer Vision*, pages 7546–7555, 2019.

[22] Weiping Liu, Jia Sun, Wanyi Li, Ting Hu, and Peng Wang. Deep learning on point clouds and its application: A survey. *Sensors*, 19(19):4188, 2019.

[23] Daniel Maturana and Sebastian Scherer. Voxnet: A 3D convolutional neural network for real-time object recognition. In *Proceedings of IEEE/RSJ International Conference on Intelligent Robots and Systems*, pages 922–928, 2015.

[24] Gonzalo Mena, David Belanger, Scott Linderman, and Jasper Snoek. Learning latent permutations with Gumbel-Sinkhorn networks. *arXiv preprint arXiv:1802.08665*, 2018.

[25] Kenta Oono and Taiji Suzuki. Graph neural networks exponentially lose expressive power for node classification. In *Proceedings of the International Conference on Learning Representations*, 2020.

[26] Pedro O Pinheiro. Unsupervised domain adaptation with similarity learning. In *Proceedings of the IEEE Conference on Computer Vision and Pattern Recognition*, pages 8004–8013, 2018.

[27] Charles R Qi, Hao Su, Kaichun Mo, and Leonidas J Guibas. PointNet: Deep learning on point sets for 3D classification and segmentation. In *Proceedings of the IEEE Conference on Computer Vision and Pattern Recognition*, pages 652–660, 2017.

[28] Charles R Qi, Li Yi, Hao Su, and Leonidas J Guibas. PointNet++: Deep hierarchical feature learning on point sets in a metric space. *arXiv preprint arXiv:1706.02413*, 2017.

[29] Siamak Ravanbakhsh, Jeff Schneider, and Barnabas Poczos. Deep learning with sets and point clouds. *arXiv preprint arXiv:1611.04500*, 2016.

[30] Vinit Sarode, Xueqian Li, Hunter Goforth, Yasuhiro Aoki, Rangaprasad Arun Srivatsan, Simon Lucey, and Howie Choset. PCRNet: Point cloud registration network using pointnet encoding. *arXiv preprint arXiv:1908.07906*, 2019.

[31] Yang-Tian Sun, Qian-Cheng Fu, Yue-Ren Jiang, Zitao Liu, Yu-Kun Lai, Hongbo Fu, and Lin Gao. Human motion transfer with 3D constraints and detail enhancement. *arXiv preprint arXiv:2003.13510*, 2020.

[32] Federico Tombari, Samuele Salti, and Luigi Di Stefano. Unique signatures of histograms for local surface description. In *Proceedings of European Conference on Computer Vision*, pages 356–369. Springer, 2010.

[33] Gül Varol, Javier Romero, Xavier Martin, Naureen Mahmood, Michael J. Black, Ivan Laptev, and Cordelia Schmid. Learning from synthetic humans. In *Proceedings of the IEEE Conference on Computer Vision and Pattern Recognition*, 2017.

[34] Weiyue Wang, Ronald Yu, Qiangui Huang, and Ulrich Neumann. SGPN: Similarity group proposal network for 3D point cloud instance segmentation. In *Proceedings of the IEEE Conference on Computer Vision and Pattern Recognition*, pages 2569–2578, 2018.

[35] Yue Wang and Justin M Solomon. Deep closest point: Learning representations for point cloud registration. In *Proceedings of the IEEE/CVF International Conference on Computer Vision*, pages 3523–3532, 2019.

[36] Yue Wang, Yongbin Sun, Ziwei Liu, Sanjay E Sarma, Michael M Bronstein, and Justin M Solomon. Dynamic graph cnn for learning on point clouds. *ACM Transactions on Graphics*, 38(5):1–12, 2019.

[37] Zonghan Wu, Shirui Pan, Fengwen Chen, Guodong Long, Chengqi Zhang, and S Yu Philip. A comprehensive survey on graph neural networks. *IEEE Transactions on Neural Networks and Learning Systems*, 32(1):4–24, 2020.

[38] Yifan Xu, Tianqi Fan, Mingye Xu, Long Zeng, and Yu Qiao. Spidercnn: Deep learning on point sets with parameterized convolutional filters. In *Proceedings of the European Conference on Computer Vision*, pages 87–102, 2018.

[39] Jiaqi Yang, Qian Zhang, Ke Xian, Yang Xiao, and Zhiguo Cao. Rotational contour signatures for both real-valued and binary feature representations of 3D local shape. *Computer Vision and Image Understanding*, 160:133–147, 2017.

[40] Jiaqi Yang, Qian Zhang, Yang Xiao, and Zhiguo Cao. Toldi: An effective and robust approach for 3D local shape description. *Pattern Recognition*, 65:175–187, 2017.

[41] Zi Jian Yew and Gim Hee Lee. RPM-Net: Robust point matching using learned features. In *Proceedings of the IEEE/CVF Conference on Computer Vision and Pattern Recognition*, pages 11824–11833, 2020.

[42] Manzil Zaheer, Satwik Kottur, Siamak Ravanbakhsh, Barnabas Poczos, Russ R Salakhutdinov, and Alexander J Smola. Deep sets. In I. Guyon, U. V. Luxburg, S. Bengio, H. Wallach, R. Fergus, S. Vishwanathan, and R. Garnett, editors, *Advances in Neural Information Processing Systems*, volume 30. Curran Associates, Inc., 2017.

[43] Andy Zeng, Shuran Song, Matthias Nießner, Matthew Fisher, Jianxiong Xiao, and Thomas Funkhouser. 3DMatch: Learning local geometric descriptors from rgb-d reconstructions. In *Proceedings of the IEEE Conference on Computer Vision and Pattern Recognition*, pages 1802–1811, 2017.

[44] Yiming Zeng, Yue Qian, Zhiyu Zhu, Junhui Hou, Hui Yuan, and Ying He. CorrNet3D: Unsupervised end-to-end learning of dense correspondence for 3D point clouds. In *Proceedings of the IEEE/CVF Conference on Computer Vision and Pattern Recognition*, pages 6052–6061, 2021.

[45] Zhiyuan Zhang, Yuchao Dai, and Jiadai Sun. Deep learning based point cloud registration: an overview. *Virtual Reality & Intelligent Hardware*, 2(3):222–246, 2020.

[46] Yu Zhong. Intrinsic shape signatures: A shape descriptor for 3D object recognition. In *Proceedings of IEEE International Conference on Computer Vision Workshops*, pages 689–696. IEEE, 2009.